Contents

Theory stuff

The $B^0 \to K^{*0} e^+ e^-$ decay proceed via a flavour-changing neutral current (FCNC) and is therefore particularly sensitive to contributions from physics beyond the Standard Model (SM). The decay is forbidden at tree-level and will proceed through higher order diagrams. New physics can manifest in the loop and cause deviations from SM predictions.
This chapter starts with a introduction into the effective theories used to describe the $B^0 \to K^{*0} l^+ l^-$ decays. This section is followed by an explication of the $b \to s\gamma$ transition which is the main contribution to the $B^0 \to K^{*0} e^+ e^-$ decay. In the framework of the SM, the photons from the $b \to s\gamma$ transition are predicted to be dominantly left-handed and therefore the measurement of a significant right-handed polarisation amplitude would be a sign for new physics.
The measurement of the photon polarisation can be performed by an angular analysis of the $B^0 \to K^{*0} l^+ l^-$ decay which is explored in Section ssec:ksll.
The advantages of using the electron-final state in $B^0 \to K^{*0} e^+ e^-$ at low invariant dilepton mass q are illustrated at the end of this chapter.

0.1 Effective Theories and effective Hamiltonian

The transitions in the $B^0 \to K^{*0} l^+ l^-$ decay are carried out by the weak interaction ($\mu \sim \mathcal{O}(m_b)$) while the binding of the quarks to mesons happens by the strong interaction ($\mu \sim \mathcal{O}(1\,\mathrm{GeV})$). Therefore the $B^0 \to K^{*0} l^+ l^-$ decay is a multi-scale process that can be described using the Effective Field Theories. Due to the strong hierarchy between external and internal scales a mathematical separation between low and high energy terms can be performed within the framework of the Operator Product Expansion (OPE) [**?**].
The effective Hamiltonian can then be expressed in terms of effective point-like vertices which are represented by the local operators $\mathcal{O}_i(\mu)$ and their associated Wilson coefficients $\mathcal{C}_i(\mu)$ which can be regarded as coupling constants associated with these effective vertices. The effective point-like vertices are introduced because Feynman diagrams such as those in Figures **??** and **??** with full W, Z^0 and t propagators only represent the interaction at very short distance scales ($\mu \sim \mathcal{O}(m_W, m_Z, m_t)$) while the long distance operators with scales of $\mu \sim \mathcal{O}(m_b)$ have to be taken into account too [**?**]. The resulting effective Hamiltonian can be expressed as

$$\mathcal{H}_{eff} = -\frac{4G_F}{\sqrt{2}} |V_{tb}||V_{ts}|^* \sum_{i=1}^{10} [\mathcal{C}_i(\mu)\mathcal{O}_i(\mu) + \mathcal{C}_i'(\mu)\mathcal{O}_i'(\mu)] \tag{1}$$

The dashed variables $\mathcal{C}_i'(\mu)$ and $\mathcal{O}_i'(\mu)$ represent the chirality-flipped Wilson coefficients and local operators respectively [**?**].
Since the energy scale in B physics is typically chosen to be $\mu \sim \mathcal{O}(m_b)$, the local operators $\mathcal{O}_i(\mu \sim \mathcal{O}(m_b))$ have to be calculated using non-perturbative methods. The Wilson coefficients on the other hand, are calculated at $\mu \sim \mathcal{O}(m_W)$ – where

perturbative techniques can be applied – up to NNLO (Next to Next to Leading Order). Renormalisation techniques are then applied to find their values at the appropriate energy scales $\mu \sim \mathcal{O}(m_b)$.

0.2 The photon polarisation in the $b \to s\gamma$ transition

The $b \to s\gamma$ transition is the main contribution to the $B^0 \to K^{*0}l^+l^-$ decay. The corresponding Feynman diagrams are shown in Figure 1.
The process can be expressed in the effective theory by the magnetic-operators [**?**] $\overline{s}_L\sigma_{\mu\nu}b_R$ and $\overline{s}_R\sigma_{\mu\nu}b_L$ which introduce the helicity structure $b_R \to s_L\gamma_L$ and $b_L \to s_R\gamma_R$. Due to the fact that the W bosons only couple to fermions of left-handed chirality, the magnetic operators are weighted with the mass of the b quark and s quark respectively $m_b\overline{s}_L\sigma_{\mu\nu}b_R$ and $m_s\overline{s}_R\sigma_{\mu\nu}b_L$.
As a result, the second process is suppressed by the factor m_s/m_b which means that the photons from the $b \to s\gamma$ transition is dominantly left-handed. Expressed in amplitudes of the photon polarisation this yields a suppression factor of $\frac{A_R}{A_L} \sim \frac{m_s}{m_b}$ (A_R: right-handed polarisation amplitude, A_L: left-handed polarisation amplitude). Taking into account additional gluon contributions in the penguin-diagram and QCD corrections, the SM prediction for the ratio of right-handed amplitude to left-handed amplitude is $\frac{A_R}{A_L} \approx 5\,\%$ [1]. Therefore a measurement of a significant right-handed amplitude is an unambiguous signal for new physics.

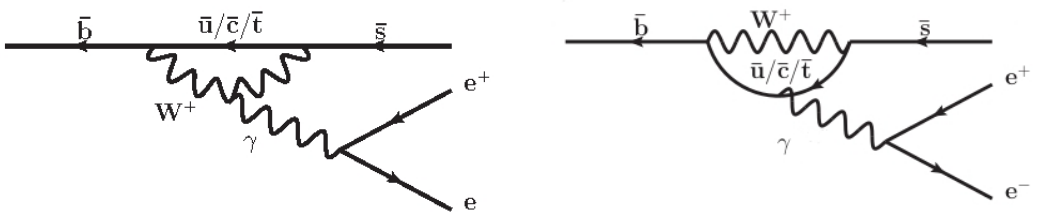

Figure 1: *The Feynman diagrams for the $b \to s\gamma$ transition.*

0.3 Angular analysis of the $B^0 \to K^{*0}e^+e^-$

While various ways to measure the photon polarisation have been presented by theorists [**?**], the most promising is the angular analysis of a decay of the form $B^0 \to K^{*0}l^+l^-$ (with $K^{*0} \to K^+\pi^-$).
This decay proceeds predominantly via the $b \to s\ell^+\ell^-$ transition with a virtual photon decaying into two leptons. Since the photon is virtual,the kinematics in the $b \to s\ell^+\ell^-$ transition are the same as in the $b \to s\gamma$ transition, particularly the helicity structure is the same.
In B decays into two vectors (here the virtual photon and the K^{*0}) the subsequent decays of the vectors contain their relative polarisation information [**?**]. Thus, the

[1] Because no *CP* violation is assumed in the $b \to s\gamma$, the statements for the $b \to s\gamma$ transition are also true for the *CP* transformed process. This means that the photons from the $\overline{b} \to \overline{s}\gamma$ transition are dominantly right-handed and $\frac{\bar{A}_L}{\bar{A}_R} \approx 5\,\%$.

angular distribution in the relative angles of the $K^{*0} \to K^+\pi^-$ decay plane and the plane of the lepton-pair can be used to determine the helicity amplitudes in the $B^0 \to K^{*0}l^+l^-$ decay and therefore the polarisation amplitudes A_R and A_L of the photon.

0.3.1 Contributions to $B^0 \to K^{*0}l^+l^-$ and the effective Hamiltonian

The $B^0 \to K^{*0}l^+l^-$ decay proceeds at low lepton-pair invariant mass predominantly via the $b \to s\ell^+\ell^-$ transition but other transitions such as the box-diagram in Figure 2 add a non-negligible contribution to the effective Hamiltonian.

The leading order contributions to the $B^0 \to K^{*0}l^+l^-$ effective Hamiltonian (see

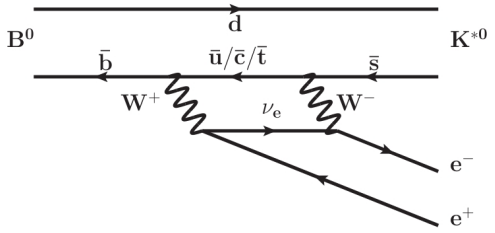

Figure 2: *The box-diagram that contributes to* $B^0 \to K^{*0}l^+l^-$

Equation 1) come from the operators $\mathcal{O}_7$, $\mathcal{O}_9$ and $\mathcal{O}_{10}$.

$$\begin{aligned}\mathcal{H}_{eff} = -\frac{4G_F}{\sqrt{2}}|V_{tb}||V_{ts}|^*[\quad & \mathcal{C}_7(\mu)\mathcal{O}_7(\mu) + \mathcal{C}'_7(\mu)\mathcal{O}'_7(\mu) \\ & \mathcal{C}_9(\mu)\mathcal{O}_9(\mu) + \mathcal{C}'_9(\mu)\mathcal{O}'_9(\mu) \\ & \mathcal{C}_{10}(\mu)\mathcal{O}_{10}(\mu) + \mathcal{C}'_{10}(\mu)\mathcal{O}'_{10}(\mu) \quad]\end{aligned} \tag{2}$$

with the local operators

$$\begin{gathered}\mathcal{O}_7 = \tfrac{e}{16\pi^2}\bar{s}\sigma_{\mu\nu}(m_b P_R \; + \; m_s P_L)bF^{\mu\nu} \\ \mathcal{O}_9 = \tfrac{e^2}{16\pi^2}(\bar{s}\gamma_\mu P_L b)(\bar{e}\gamma^\mu e) \qquad \mathcal{O}_{10} = \tfrac{e^2}{16\pi^2}(\bar{s}\gamma_\mu P_L b)(\bar{e}\gamma^\mu\gamma_5 e)\end{gathered} \tag{3}$$

The $\mathcal{O}_7$ corresponds to the SM $b \to s\ell^+\ell^-$ transition ($b \to s\gamma$ transition) with a left-handed weak-charged current. Since there are no right-handed weak-charged currents in the SM, the $\mathcal{C}'_{7(\mu)}$ is only non-zero for contributions from new physics. It is therefore appreciable to measure quantities connected to $\mathcal{C}'_7$.

The operators $\mathcal{O}_9$ and $\mathcal{O}_{10}$ represent the contribution to the $B^0 \to K^{*0}l^+l^-$ decay that do not come from the $b \to s\gamma$ transition but for example from the box-diagram in Figure 2.

The branching ratio $\mathcal{B}(b \to s\gamma)$ is anti-proportional to square of the lepton-pair invariant mass q^2 while the branching ratio of the other contributions shows no significant q^2 dependences. The latter make up for about 7% of the events with $30\,\text{MeV} < q < 1\,\text{GeV}$.

At LHCb the angular analysis of $B^0 \to K^{*0}l^+l^-$ decays is performed with muons and electron in different bins of q. The combination of these analyses gives global

information about all polarisation amplitudes over a large range of q and the relative contributions from $\mathcal{C}_9(\mu)$ and $\mathcal{C}_{10}(\mu)$ can be determined.

0.3.2 Polarisation amplitudes for the $B^0 \to K^{*0}e^+e^-$

In the framework of the effective theory, the transversity polarisation amplitudes $A_\perp^{L,R}$, $A_\parallel^{L,R}$ and $A_0^{L,R}$ can be expressed in terms of the Wilson coefficients. The indices L and R refer to the chirality of the lepton current. In this calculation the leptons are presumed to be massless which is a very good approximation for the $B^0 \to K^{*0}e^+e^-$. As can be seen in the following formulae, the polarisation amplitudes are sensitive to new physics that might appear in the Wilson coefficients.

$$A_\perp^{L,R}(q^2) = \frac{\sqrt{2}N(M_B^2 - q^2)}{M_B}[(\mathcal{C}_9 + \mathcal{C}_9^{'}) \mp (\mathcal{C}_{10} + \mathcal{C}_{10}^{'}) + \frac{2m_b M_B}{q^2}(\mathcal{C}_7 + \mathcal{C}_7^{'})]\xi_\perp(q^2) \quad (4)$$

$$A_\parallel^{L,R}(q^2) = \frac{\sqrt{2}N(M_B^2 - q^2)}{M_B}[(\mathcal{C}_9 + \mathcal{C}_9^{'}) \mp (\mathcal{C}_{10} + \mathcal{C}_{10}^{'}) + \frac{2m_b M_B}{q^2}(\mathcal{C}_7 - \mathcal{C}_7^{'})]\xi_\perp(q^2) \quad (5)$$

$$A_0^{L,R}(q^2) = \frac{\sqrt{2}N(M_B^2 - q^2)}{M_B}[(\mathcal{C}_9 + \mathcal{C}_9^{'}) \mp (\mathcal{C}_{10} + \mathcal{C}_{10}^{'}) + \frac{2m_b}{M_B}(\mathcal{C}_7 - \mathcal{C}_7^{'})]\xi_\parallel(q^2) \quad (6)$$

In the above formulae $\lambda = M_B^4 + M_{K^{*0}}^4 + q^2 - 2(M_B^2 M_{K^{*0}}^2 + M_{K^{*0}}^2 q + M_B^2 q)$ and

$$N = \left[\frac{G_F^2 \alpha^2}{3 \cdot 2^{10}\pi^5 M_B^3}||V_{tb}||V_{ts}|^*|^2 q\lambda^{1/2}\Big(1 - \frac{4m_l^2}{q}\Big)^{1/2}\right] \quad (7)$$

and M_B: mass of the B meson, $M_{K^{*0}}$: mass of the K^{*0} meson, m_b: mass of the b quark. The $\xi_\perp(q^2)$ and $\xi_\parallel(q^2)$ factors are the form factors of the K^{*0} meson.
The amplitudes can also be expressed in the helicity basis where the polarisation amplitudes are

$$F_L(q^2) = \frac{|A_0^L|^2 + |A_0^R|^2}{|A_0^L|^2 + |A_\perp^L|^2 + |A_\parallel^L|^2 + |A_0^R|^2 + |A_\perp^R|^2 + |A_\parallel^R|^2} \quad (8)$$

$$A_{FB}(q^2) = \frac{3}{2}\frac{\Re(A_\parallel^L(A_\perp^L)^*) - \Re(A_\parallel^R(A_\perp^R)^*)}{|A_0^L|^2 + |A_\perp^L|^2 + |A_\parallel^L|^2 + |A_0^R|^2 + |A_\perp^R|^2 + |A_\parallel^R|^2} \quad (9)$$

$$A_T^{(2)}(q^2) = \frac{|A_\perp^L + A_\perp^R|^2 - |A_\parallel^L + A_\parallel^R|}{|A_\perp^L + A_\perp^R|^2 + |A_\parallel^L + A_\parallel^R|} \quad (10)$$

$$A_T^{Im}(q^2) = \frac{2\Im(A_\parallel^L(A_\perp^L)^* + A_\parallel^R(A_\perp^R)^*)}{|A_\perp^L + A_\perp^R|^2 + |A_\parallel^L + A_\parallel^R|} \quad (11)$$

The advantage of using the helicity amplitudes is, that especially for the $A_T^{(2)}(q^2)$ and the $A_T^{Im}(q^2)$ don't depend on the hadronic form factor $\xi_\perp(q^2)$ any more, thus a

great systematic uncertainty from the theoretical part is removed.
For the low invariant dilepton mass limit $q^2 \to 0$ the contributions from the Wilson coefficients $\mathcal{O}_9$ and $\mathcal{O}_{10}$ become negligible and the amplitude $A_T^{(2)}(q^2)$ can be simplified to

$$A_T^{(2)}(q^2 \to 0) = \frac{2\Re(\mathcal{C}_7\,(\mathcal{C}_7')^*)}{|\mathcal{C}_7|^2 + |(\mathcal{C}_7')^*|^2} = 2\,\frac{A_R}{A_L} \tag{12}$$

This shows clearly that while all amplitudes are of interest to particle physics, the variable $A_T^{(2)}(q^2)$ is the one that contains the most information about the photon polarisation.

0.3.3 Angular distribution

The $B^0 \to K^{*0} l^+ l^-$ decay is completely defined by four independent kinematic variables; namely the lepton-pair invariant mass q and the three angles θ_l, θ_K and Φ which are illustrated in Figure 3. The angles are defined as:

- θ_l: the angle between the direction of the vector of the e^+ (e^-) in the dilepton rest frame, and the direction of the dilepton in the B^0 ($\bar{B}^0$) rest frame

- θ_K: the angle between the direction of the vector of the K in the K^{*0} (K^{*0}) rest frame, and the direction of the K^{*0} (K^{*0}) in the B^0 ($\bar{B}^0$) rest frame

- Φ: the angle between the planes defined by the K^{*0} daughters and the dileption daughters, in the rest frame of the B meson.

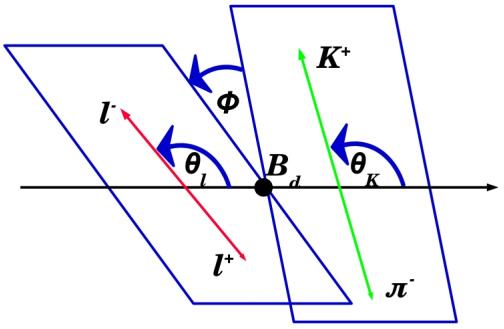

Figure 3: *Definition of the angles θ_l, θ_K and Φ in the $B^0 \to K^{*0} l^+ l^-$ decay.*

The normalized differential decay width can be expressed as

$$\frac{1}{\Gamma}\frac{d^4\Gamma}{dq\,\cos\theta_l\,\cos\theta_K\,d\Phi} = \frac{9}{32\pi}\sum_{i=1}^{9} I_i'(q,\theta_K) f_i(\theta_l,\Phi) \tag{13}$$

where the I_i' depend on q^2, θ_K and the helicity polarisation amplitudes $F_L(q^2)$, $A_{FB}(q^2)$, $A_T^{(2)}(q^2)$ and $A_T^{Im}(q^2)$. The f_i are the corresponding angular distribution functions

$$\begin{aligned}
f_1 &= 1 & f_2 &= cos(2\theta_l) & f_3 &= sin^2(\theta_l)cos(2\Phi) \\
f_4 &= sin(2\theta_l)cos(\Phi) & f_5 &= sin(\theta_l)cos(\Phi) & f_6 &= cos(\theta_l) \\
f_7 &= sin(\theta_l)sin(\Phi) & f_8 &= sin(2\theta_l)sin(\Phi) & f_9 &= sin^2(\theta_l)sin(2\Phi)
\end{aligned} \tag{14}$$

The I_is sensitive to the ratio of photon polarisations $\frac{A_R}{A_L}$ and therefore to new physics are I_3 and I_9. The partial decay width can then be simplified without any loss in information about the photon polarisation by folding the angular distributions for Φ and θ_l. Φ is folded by moving all values with $\Phi < 0$ to $\Phi + \pi$. This removes the terms proportional to $cos(\Phi)$ and $sin(\Phi)$ without affecting the $cos(2\Phi)$ and $sin(2\Phi)$ terms. The angle θ_l is folded by mapping the interval $(\pi/2, \pi)$ onto $(0, \pi/2)$ which removes the term proportional to $cos(\theta_l)$. The decay with after this transformations is

$$\begin{aligned}\frac{1}{\Gamma}\frac{d^4\,\Gamma}{dq\,\cos\theta_l\,\cos\theta_K\,d\Phi} = \frac{9}{32\pi}[&I_1'(q^2, cos\theta_K)\ + I_2'(q^2, cos\theta_K)\,cos2\theta_l \\ &+I_3'(q^2, cos\theta_K)\,sin^2\theta_l\,cos2\Phi\ + I_9'(q^2, cos\theta_K)\,sin^2\theta_l\,sin2\Phi]\end{aligned} \tag{15}$$

The I_i' terms for the particular case of $B^0 \to K^{*0}e^+e^-$– that is $m_{electron} << q$ – can be expressed as

$$\begin{aligned} I_1'(q^2, cos\theta_K) &= \frac{3}{4}(1 - F_L(q^2)) \cdot (1 - cos^2\theta_K) + F_L(q^2) \cdot cos^2\theta_K \\ I_2'(q^2, cos\theta_K) &= \frac{1}{4}(1 - F_L(q^2)) \cdot (1 - cos^2\theta_K) - F_L(q^2) \cdot cos^2\theta_K \\ I_3'(q^2, cos\theta_K) &= \frac{1}{2}(1 - F_L(q^2)) \cdot A_T^{(2)}(q^2) + (1 - cos^2\theta_K) \\ I_9'(q^2, cos\theta_K) &= \frac{1}{2}(1 - F_L(q^2)) \cdot A_T^{Im}(q^2) + (1 - cos^2\theta_K) \end{aligned} \tag{16}$$

By performing an angular analysis, all three remaining amplitudes $F_L(q^2)$, $A_T^{(2)}(q^2)$ and $A_T^{Im}(q^2)$ can be fitted at the same time and the information about the photon polarisation can be extracted.

0.3.4 The advantages of the low q^2 bin in $B^0 \to K^{*0}e^+e^-$

This masters thesis is part of an angular analysis that focusses on the low dilepton invariant mass q region in the $B^0 \to K^{*0}e^+e^-$ decay.
The choice of performing the analysis with electrons as opposed to with muons is, that the sensitivity on new physics is increased. This is due to the fact, that the electron mass is negligible compared to q^2 $m_e^2 << q^2$. For a non-negligible lepton mass the I_3' and I_9' in Equations 17 are multiplied by $\frac{1-x}{1+x/2}$ with $x = \frac{4m_e^2}{q^2}$ which degrades the sensitivity on $A_T^{(2)}(q^2)$ and $A_T^{Im}(q^2)$.
The choice of $30\,\text{MeV} < q < 1\,\text{GeV}$ has two distinct advantages. The first advantage is that the contribution coming from the non-$b \to s\ell^+\ell^-$ transitions in $\mathcal{O}_9$ and $\mathcal{O}_{10}$ are very small (about 7%) and $A_T^{(2)}(q^2) = 2\,\frac{A_R}{A_L}$ (see Section 0.3.2). The analysis of the $B^0 \to K^{*0}e^+e^-$ decay at low q^2 is therefore directly sensitive to the $b \to s\ell^+\ell^-$ transitions and the photon polarisation. The second advantage of constraining the the dilepton invariant mass lies in the q^2 dependence of the $F_L(q^2)$ amplitude shown in Figure **??**. $F_L(q^2)$ is low for small q^2 values and increases with q^2. Since the amplitude $A_T^{(2)}(q^2)$ appears in I_3' in Equation 17 in combination with $(1 - F_L(q^2))$ the sensitivity to $A_T^{(2)}(q^2)$ is highest for low q^2.
The effects of the low lepton mass of the electrons opposed to muons combined with the effects of q^2 on $F_L(q^2)$ are shown in Figure **??**.

Bibliography

[1] 35th International Confer ence of High Ener gy Physics - ICHEP2010. *Performance of the Tracking System at the LHCb Experiment*, December 2010.

[2] R. Aaij et al. Search for the rare decays $B_s^0 \to \mu^+\mu^-$ and $B^0 \to \mu^+\mu^-$. CERN-PH-EP-2011-029, April 2011.

[3] G. Barrand, I. Belyaev, et al. GAUDI- A Software Architecture and Framework for building HEP Data Processing Applications. *Computer Physics Communications*, 140(1-2), October 2001.

[4] G ; Felici G ; Murtas F ; Valente P ; Bonivento W (INFN Cagliari) ; Cardini A (INFN Cagliari) ; Lai A (INFN Cagliari) ; Pinci D (INFN Cagliari ; Cagliari U.) ; Saitta B (INFN Cagliari ; Cagliari U.) ; Bosio C (INFN Rome) Bencivenni. A triple-GEM detector with pad readout for the inner region of the first LHCb muon station. LHCb-MUON 2001-05, June 2001.

[5] The LHCb Collaboration. The DAVINCI Project. LHCb-DaVinci.

[6] The LHCb Collaboration. LHCb letter of intent. CERN/LHCC-95-5, August 1995.

[7] The LHCb Collaboration. LHCb Calorimeters Technical Design Report. Technical report, The LHCb Collaboration, September 2000.

[8] The LHCb Collaboration. LHCb Magnet Technical Design Report. Technical report, The LHCb Collaboration, January 2000.

[9] The LHCb Collaboration. LHCb RICH Technical Design Report. Technical report, The LHCb Collaboration, September 2000.

[10] The LHCb Collaboration. LHCb Muon SystemTechnical Design Report. Technical report, The LHCb Collaboration, May 2001.

[11] The LHCb Collaboration. LHCb Outer Tracker Technical Design Report. Technical report, The LHCb Collaboration, September 2001.

[12] The LHCb Collaboration. LHCb Vertex Locator Technical Design Report. Technical report, The LHCb Collaboration, May 2001.

[13] The LHCb Collaboration. LHCb Inner Tracker Technical Design Report. Technical report, The LHCb Collaboration, November 2002.

[14] The LHCb Collaboration. LHCb Trigger SystemTechnical Design Report. Technical report, The LHCb Collaboration, September 2003.

[15] The LHCb Collaboration. The LHCb detector at the LHC. Technical report, The LHCb Collaboration, 2008.

[16] V.N Ivanchenko. Geant4 toolkit for simulation of HEP experiments. *Nuclear Instruments and Methods in Physics Research Section A: Accelerators, Spectrometers, Detectors and Associated Equipment*, 502(2-3), April 2003.

[17] W.R. Leo. *Techniques for Nuclear and Particle Physics Experiements*. Springer-Verlag Berlin Heidelberg New York, 1987.

[18] Pablo RodrÃÂguez PÃÂ©rez, for the LHCb VELO Group, and for the VELO Upgrade group. The LHCb Vertex Locator performance and Vertex Locator upgrade, October 2012.

[19] Anders Ryd, David Lange, et al. EvtGen, A Monte Carlo Generator for B -Physics. EvtGen V00-11-06, February 2004.

[20] Torbjorn Sjostrand, Stephen Mrenna, and Peter Skands. PYTHIA 6.4 Physics and Manual. *JHEP 0605:026,2006*, May 2006.